

A Resolved Millimeter Emission Belt in the AU Mic Debris Disk

David J. Wilner¹, Sean M. Andrews¹, Meredith A. MacGregor¹, A. Meredith Hughes²

ABSTRACT

We present imaging observations at 1.3 millimeters of the debris disk surrounding the nearby M-type flare star AU Mic with beam size $3''$ (30 AU) from the Submillimeter Array. These data reveal a belt of thermal dust emission surrounding the star with the same edge-on geometry as the more extended scattered light disk detected at optical wavelengths. Simple modeling indicates a central radius of ~ 35 AU for the emission belt. This location is consistent with the reservoir of planetesimals previously invoked to explain the shape of the scattered light surface brightness profile through size-dependent dust dynamics. The identification of this belt further strengthens the kinship between the debris disks around AU Mic and its more massive sister star β Pic, members of the same ~ 10 Myr-old moving group.

Subject headings: circumstellar matter — planet-disk interactions — stars: individual (AU Microscopii) — submillimeter: planetary systems

1. Introduction

AU Mic is a nearby (9.91 ± 0.10 pc, van Leeuwen 2007) M1Ve flare star (Torres et al. 2006) with the young age of 12^{+8}_{-4} Myr (Zuckerman et al. 2001), a key epoch in the formation of planetary systems. The star is surrounded by a nearly edge-on circumstellar disk discovered in coronagraphic images of scattered starlight that extends to a radius of at least 210 AU (Kalas et al. 2004). Since the small grains responsible for scattering should be removed rapidly by stellar pressure forces, the disk is thought to consist of the collisional debris of unseen planetesimals experiencing ongoing impacts (for recent reviews of the debris disk

¹Harvard-Smithsonian Center for Astrophysics, 60 Garden Street, Cambridge, MA 02138

²Department of Astronomy, 601 Campbell Hall, University of California, Berkeley, CA 94720

phenomenon, see Wyatt 2008; Krivov 2010). Because of its proximity, the AU Mic debris disk has become one of the best studied examples at optical and infrared wavelengths, including detailed imagery of both intensity and polarization from the *Hubble Space Telescope* (Krist et al. 2005; Graham et al. 2007).

Many observational properties of the AU Mic debris disk bear striking similarities to the archetype debris disk surrounding β Pic, also viewed nearly edge-on and located in the same young moving group. In particular, the midplane optical surface brightness profiles of these disks are remarkably alike, with shallow inner slopes ($\sim 1/r^{1-2}$) that steepen substantially ($\sim 1/r^{4-5}$) in the outer regions, near 35 AU and 100 AU for AU Mic and β Pic, respectively (Krist et al. 2005; Fitzgerald et al. 2007; Heap et al. 2000; Golimowski et al. 2006). These similarities inspired the development of a unified framework for debris disks based on a localized belt of planetesimals, or “birth ring”, that produces dust in a collisional cascade (Strubbe & Chiang 2006; Augereau & Beust 2006). The smallest grains are blown out from the belt by radiation and winds from the star, larger grains are launched into eccentric orbits with the same periastron as the belt, and the largest grains, which are minimally affected by non-gravitational forces, do not travel far from the belt before being ground down. The grains are therefore segregated according to their size, which gives rise to the characteristic scattered light profile. For these dynamics to prevail, the disks must be substantially free of gas (Thébaud & Augereau 2005), a property confirmed by measurements at ultraviolet wavelengths (Roberge et al. 2005; France et al. 2007).

A “birth ring”, if present, would remain hidden in optical and infrared images dominated by small grains that populate an extended halo (e.g., Su et al. 2005). By contrast, observations at (sub)millimeter wavelengths highlight thermal emission from the largest grains and hence the location of the dust-producing planetesimals (Wyatt 2006). To date, the best case for a “birth ring” comes from millimeter observations of β Pic (Wilner et al. 2011). While the optical disk of β Pic extends more than 1000 AU from the star, the millimeter imaging reveals a much more compact belt of emission at ~ 95 AU radius. This millimeter emission belt coincides with the change in the slope of the optical surface brightness, which in the models marks the outer extent of the colliding planetesimals.

Previous (sub)millimeter-wave observations of AU Mic did not have sufficient angular resolution to reveal much about the emission morphology. A detection at $850 \mu\text{m}$ using JCMT/SCUBA ($14''$ beam) indicated a reservoir of cold dust with mass $\sim 0.01 M_{\oplus}$, but did not resolve any structure (Liu et al. 2004). Subsequent observations at $350 \mu\text{m}$ using CSO/SHARC II ($10''$ beam) marginally resolved an orientation compatible with the scattered light, but were otherwise limited (Chen et al. 2005). In this *Letter*, we present imaging

observations of AU Mic at 1.3 millimeters using the Submillimeter Array (SMA)¹ that obtain 3'' resolution and provide evidence for a planetesimal belt.

2. Observations

We observed AU Mic with the SMA (Ho et al. 2004) on Mauna Kea, Hawaii at 1.3 millimeters wavelength using the compact and extended configurations of the array. Table 1 provides basic information about these observations, including the observing dates, baseline lengths, and atmospheric opacities. The weather conditions were good for all of these observations and best for the two compact configuration tracks when only 6 of the 8 array antennas were available. The phase center was $\alpha = 20^h 45^m 09^s.53$, $\delta = -31^\circ 20' 27''.2$ (J2000), offset by $\sim 5''.3$ from the location of the star. The $\sim 54''$ (FWHM) field of view is set by the primary beam size of the 6 meter diameter array antennas. The total bandwidth available was 8 GHz derived from two sidebands spanning ± 4 to 8 GHz from the LO frequency. Time dependent complex gains were calibrated using observations of two quasars, J2101-295 (3.9 degrees away) and J1924-292 (17.4 degrees away), interleaved with observations of AU Mic in a 15 minute cycle. The passband shape for each track was calibrated using available bright sources, mainly J1924-292. The absolute flux scale was set with an accuracy of $\sim 10\%$ using observations of Callisto or Ganymede in each track. All of the calibration steps were performed using the IDL based MIR software, and imaging and deconvolution were done with standard routines in the MIRIAD package. We made a series of images with a wide range of visibility weighting schemes to explore compromises between higher angular resolution and better surface brightness sensitivity.

3. Results and Analysis

3.1. 1.3 Millimeter Emission

Figure 1 shows a contour image of the 1.3 millimeter emission overlaid on a *Hubble Space Telescope*/ACS coronagraphic image of optical scattered light (F606W filter) from Graham et al. (2007). The synthesized beam size for this 1.3 millimeter image is $3''.3 \times 2''.6$ (33×26 AU), position angle -12° , obtained with natural weighting and an elliptical Gaussian

¹The Submillimeter Array is a joint project between the Smithsonian Astrophysical Observatory and the Academia Sinica Institute of Astronomy and Astrophysics and is funded by the Smithsonian Institution and the Academia Sinica.

taper $1''.5 \times 1''.0$ (FWHM) oriented east-west to make the beam shape more circular. The rms noise in this image is $0.40 \text{ mJy beam}^{-1}$, and the individual peaks have a signal-to-noise $\gtrsim 7$. The star symbol marks the stellar position corrected for proper motion, offset by $(3''.20, -4''.25)$ from the phase center. The image shows a resolved band of 1.3 millimeter emission that extends approximately symmetrically from the stellar position to the southeast and northwest. By fitting a line to the positions of the two peaks in the image, we estimate the position angle of the emission structure to be $130 \pm 2^\circ$, in excellent agreement with the disk orientation inferred from scattered light observations (Liu 2004). From its position angle and double peaked morphology, we identify the emission structure as a limb-brightened dust belt. Note that thermal emission from the stellar photosphere contributes only 0.06 mJy at this wavelength, and even the strongest synchrotron radio flares from stellar activity should remain well below the noise (Kundu et al. 1987). The total flux density obtained by integrating over a box that surrounds the emission is $8.5 \pm 2 \text{ mJy}$, where the uncertainty is estimated conservatively by evaluating boxes of the same size in emission-free regions of the image. No other significant features are detected in the field of view.

An extrapolation of the measurements at shorter wavelengths indicates that missing flux due to the spatial filtering by the SMA is not a significant issue for these observations. The spectral index between $350 \mu\text{m}$ (Chen et al. 2005) and $850 \mu\text{m}$ (Liu et al. 2004) is $1.7_{-0.5}^{+0.3}$, which predicts $7.1_{-1.2}^{+2.0} \text{ mJy}$ at 1.3 millimeters, in good agreement with the SMA measurement. This shallow index is consistent, within the uncertainties, with values near 2.0 determined for a sample of debris disks by Gáspár et al. (2011), notably for stars later than F-type where dust temperatures are so low that the Rayleigh-Jeans approximation in this part of the spectrum is invalid. We conclude that the compact structure detected by the SMA accounts for all of the 1.3 millimeter emission in the AU Mic system.

3.2. A Simple Disk Model

To characterize the millimeter emission structure, we use a simple parametric disk model, following closely the method used by Wilner et al. (2011) for analyzing similar observations of the β Pic disk. We assume the emission arises from a geometrically thin, axisymmetric belt with a radial surface brightness profile given by $I \propto f(r)r^{-q}$. This functional form is intended to capture the essence of low optical depth emission from a disk with a spatially invariant dust emissivity, surface density profile $f(r)$, and temperature profile that falls off with radius as a power-law. We fix the power-law index $q = 0.5$ to approximate radiative heating from the central star, and we consider two shapes for $f(r)$: (1) an annulus with power law slope, $f(r) \propto r^{-p}$ for $R \pm \Delta R/2$, $p \in 0, 1$, and (2) a Gaussian, $f(r) \propto \exp[-((r - R)/\sqrt{2}\Delta R)^2]$.

In each case, the model is described by three parameters: a center radius R , width ΔR , and total flux density $F = \int I d\Omega$. We fix the disk inclination at 89.5° and position angle at 130° , as determined from scattered light data (Krist et al. 2005), and place the origin within $0''.1$ of the nominal stellar position (within the SMA astrometric accuracy). Note that the vertical thickness of the millimeter grain population is expected to be $< 0''.25$ (Thébaud 2009), negligible compared to the resolution of the data. The utility of this simple modeling approach is to provide basic constraints while avoiding the multitudinous assumptions about grain properties, dynamics, and radiative transfer required in more sophisticated treatments.

To estimate the model parameters and their uncertainties, we calculate three-dimensional grids spanning appropriate ranges of the parameter values. For the Gaussian model, the grid covers $20 < R < 47$ AU and $1 < \Delta R < 40$ AU in 1 AU steps, and $5 < F < 11$ mJy in 0.2 mJy steps. For each position in a model grid, we compute a set of synthetic SMA visibilities and compare directly to the data with a χ^2 value (the sum of real and imaginary components over all spatial frequencies) that uses natural weights modified by the Gaussian taper used for the image in Figure 1. The rightmost panel of Figure 2 shows the χ^2 surface in the $(R, \Delta R)$ plane for the Gaussian model after marginalizing over F . The best-fit model is marked by a cross, and the contours delineate (marginalized) 1σ intervals in $\Delta\chi^2$. The best-fit center radius is $R = 36_{-16}^{+7}$ AU, with corresponding width $\Delta R = 10_{-8}^{+13}$ AU (or $\text{FWHM} = 2\sqrt{2\ln 2}\Delta R = 23_{-19}^{+31}$ AU) and flux density $F = 8.0 \pm 1.2$ mJy. The three lefthand panels of Figure 2 show the original 1.3 millimeter image from Figure 1, the Gaussian model image obtained using the best-fit parameter values and the same visibility weighting scheme, and the imaged residuals (where data–model subtraction is conducted on the visibilities). This comparison shows clearly that the best-fit model reproduces the main features of the image and leaves no systematic residuals. The power-law models for $f(r)$ give similar best-fit parameter values: for $p = 0$, we find $R = 35 \pm 6$ AU and $\Delta R = 38_{-18}^{+26}$ AU (where the upper limit is set by the computational grid boundary). For $p = 1$, the best-fit locus is shifted to roughly 10% larger values of R , a manifestation of the degeneracy between the radial gradient and emission extent. All of these best-fit models reproduce the observed SMA visibilities equally well (i.e., have effectively the same minimum χ^2 values).

The modest signal-to-noise of the observations preclude placing tighter constraints on the model parameters. Nonetheless, it is reassuring that consistent results are obtained from the various assumptions about the emission morphology. Each gives a similar center radius, as well as an effectively cleared central cavity with size compatible with that inferred from scattered light (~ 12 AU Krist et al. 2005) and the lack of mid-infrared emission (~ 17 AU Liu et al. 2004). The best-fit Gaussian model reproduces better the contrast of the maxima to the extended emission of the disk in the image plane, but there is no clear preference for any of the functional forms. Of course, none of these *ad hoc* models are perfect, and more

sensitive data will be needed to constrain further the details of the emission distribution.

4. Discussion

We have spatially resolved the thermal emission at 1.3 millimeters from the AU Mic debris disk, thereby revealing the distribution of its millimeter grain population. These large grains are expected to have dynamics similar to the unseen dust-producing planetesimals, and the emission at this long wavelength provides a direct link to their spatial distribution.

The overall structure of the AU Mic millimeter emission is reproduced well by a belt surrounding the star centered near a radius of 35 AU. The inferred location of this emission belt coincides with the region over which the scattered light brightness profile of the disk steepens markedly, the feature that provided impetus for developing the “birth ring” model. Like AU Mic’s more massive sister star β Pic (Wilner et al. 2011), the resolved multi-wavelength data are consistent with a scenario where destructive collisions of planetesimals within the belt create grains with a spectrum of sizes, and the effects of size-dependent dust dynamics generate the millimeter emission and spatially extended scattered light nebula. For β Pic, the intense stellar radiation pressure can account for the large halo of small grains in the outer disk. But for AU Mic, which is about two orders of magnitude less luminous, the much weaker stellar radiation field is apparently augmented by a stellar wind to expel small grains (Strubbe & Chiang 2006; Augereau & Beust 2006).

Though the fractional radial extent of the AU Mic millimeter emission is not strongly constrained, the best-fit models suggest that it could be broad, $\Delta R/R \sim 1$. For β Pic, the millimeter emission is characterized by $\Delta R/R < 0.5$, with the upper end favored for the width of the underlying dust-producing planetesimal belt from detailed models of the knee of the scattered light profile (Hahn 2010). Such broad belts are not unusual features of debris disks, in particular among the few resolved at millimeter wavelengths (Hughes et al. 2011). An inner cavity devoid of dust is plausibly maintained by the combination of grinding collisions in the belt and clearing by stellar radiation forces, though a tenable alternative is that the inner regions are swept clear by a planet. Planets seem to be the most viable explanation for the millimeter cavities common to the gas-rich transition disks around younger, pre-main-sequence stars (Andrews et al. 2011). While a planet has been imaged to orbit within the cavity in the disk around β Pic (Lagrange et al. 2010), direct evidence for planets in the AU Mic system remains elusive, both from high contrast imaging observations (Masciadri et al. 2005; Metchev et al. 2005) and from transit searches (Hebb et al. 2007). The outer boundary of the emission belts may reflect the outer extent of successful planetesimal formation, or it may simply mark the edge of the region where the planetesimal stirring mechanism has

been successful at initiating dust-producing collisions, as in the models of Kenyon & Bromley (2004).

These new millimeter observations of AU Mic show the global structure of large grains in its debris disk, but they do not have sufficient resolution and sensitivity to reveal any significant departures from axisymmetry or substructure that might result from gravitational interactions with unseen planets. The higher resolution images of scattered light clearly show several radial and vertical inhomogeneities at subarcsecond scales (features A-E, see Liu 2004; Metchev et al. 2005; Fitzgerald et al. 2007). If these substructures have counterparts at millimeter wavelengths, then future observations with the Atacama Large Millimeter/Submillimeter Array (ALMA) may be able to detect them, pinpoint the location of parent bodies, and constrain their origins.

We thank James Graham for providing the *Hubble Space Telescope* image in Figure 1. A. M. H. is supported by a fellowship from the Miller Institute for Basic Research in Science.

Facility: Submillimeter Array

REFERENCES

- Andrews, S. M., Wilner, D. J., Espaillat, C., et al. 2011, *ApJ*, 732, 42
- Augereau, J.-C., & Beust, H. 2006, *A&A*, 455, 987
- Chen, C. H., Patten, B. M., Werner, M. W., et al. 2005, *ApJ*, 634, 1372
- Fitzgerald, M. P., Kalas, P. G., Duchêne, G., Pinte, C., & Graham, J. R. 2007, *ApJ*, 670, 536
- France, K., Roberge, A., Lupu, R. E., Redfield, S., & Feldman, P. D. 2007, *ApJ*, 668, 1174
- Gáspár, A., Psaltis, D., Rieke, G. H., & Oumlzel, F. 2011, arXiv:1111.0296
- Golimowski, D. A., Ardila, D. R., Krist, J. E., et al. 2006, *AJ*, 131, 3109
- Graham, J. R., Kalas, P. G., & Matthews, B. C. 2007, *ApJ*, 654, 595
- Hahn, J. M. 2010, *ApJ*, 719, 1699
- Heap, S. R., Lindler, D. J., Lanz, T. M., et al. 2000, *ApJ*, 539, 435
- Hebb, L., Petro, L., Ford, H. C., et al. 2007, *MNRAS*, 379, 63

- Ho, P. T. P., Moran, J. M., & Lo, K. Y. 2004, *ApJ*, 616, L1
- Hughes, A. M., Wilner, D. J., Andrews, S. M., et al. 2011, *ApJ*, 740, 38
- Kalas, P., Liu, M. C., & Matthews, B. C. 2004, *Science*, 303, 1990
- Kenyon, S. J., & Bromley, B. C. 2004, *AJ*, 127, 513
- Krist, J. E., Ardila, D. R., Golimowski, D. A., et al. 2005, *AJ*, 129, 1008
- Krivov, A. V. 2010, *Research in Astronomy and Astrophysics*, 10, 383
- Kundu, M. R., Jackson, P. D., White, S. M., & Melozzi, M. 1987, *ApJ*, 312, 822
- Lagage, P. O., & Pantin, E. 1994, *Nature*, 369, 628
- Lagrange, A.-M., Bonnefoy, M., Chauvin, G., et al. 2010, *Science*, 329, 57
- Liu, M. C. 2004, *Science*, 305, 1442
- Liu, M. C., Matthews, B. C., Williams, J. P., & Kalas, P. G. 2004, *ApJ*, 608, 526
- Masciadri, E., Mundt, R., Henning, T., Alvarez, C., & Barrado y Navascués, D. 2005, *ApJ*, 625, 1004
- Metchev, S. A., Eisner, J. A., Hillenbrand, L. A., & Wolf, S. 2005, *ApJ*, 622, 451
- Roberge, A., Weinberger, A. J., Redfield, S., & Feldman, P. D. 2005, *ApJ*, 626, L105
- Su, K. Y. L., Rieke, G. H., Misselt, K. A., et al. 2005, *ApJ*, 628, 487
- Strubbe, L. E., & Chiang, E. I. 2006, *ApJ*, 648, 652
- Thébaud, P., & Augereau, J.-C. 2005, *A&A*, 437, 141
- Thébaud, P. 2009, *A&A*, 505, 1269
- Torres, C. A. O., Quast, G. R., da Silva, L., et al. 2006, *A&A*, 460, 695
- van Leeuwen, F. 2007, *A&A*, 474, 653
- Vidal-Madjar, A., Lagrange-Henri, A.-M., Feldman, P. D., et al. 1994, *A&A*, 290, 245
- Wilner, D. J., Andrews, S. M., & Hughes, A. M. 2011, *ApJ*, 727, L42
- Wyatt, M. C. 2006, *ApJ*, 639, 1153

Wyatt, M. C. 2008, *ARA&A*, 46, 339

Zuckerman, B., Song, I., Bessell, M. S., & Webb, R. A. 2001, *ApJ*, 562, L87

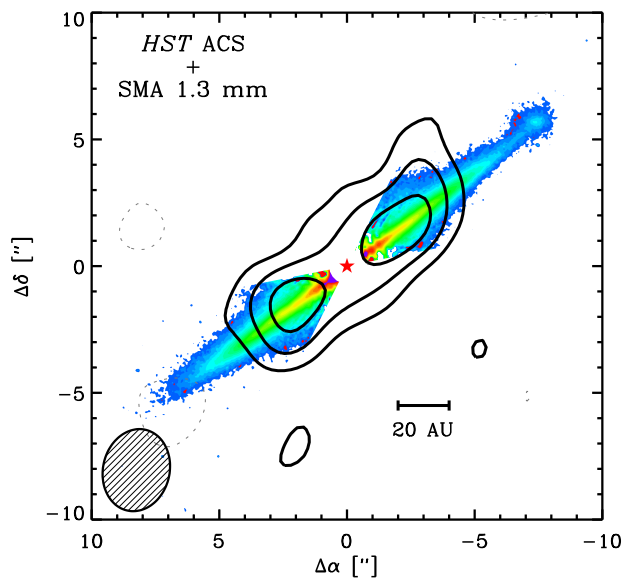


Fig. 1.— SMA image of the 1.3 millimeter continuum emission from AU Mic, overlaid on an image of optical scattered light from the *Hubble Space Telescope* (Graham et al. 2007). The contour levels are $-2, 2, 4, 6 \times 0.40$ mJy (the rms noise level); negative contours are dotted. The ellipse in the lower left corner represents the $3''.3 \times 2''.6$ (FWHM) synthesized beam size. The star symbol indicates the location of the stellar photosphere.

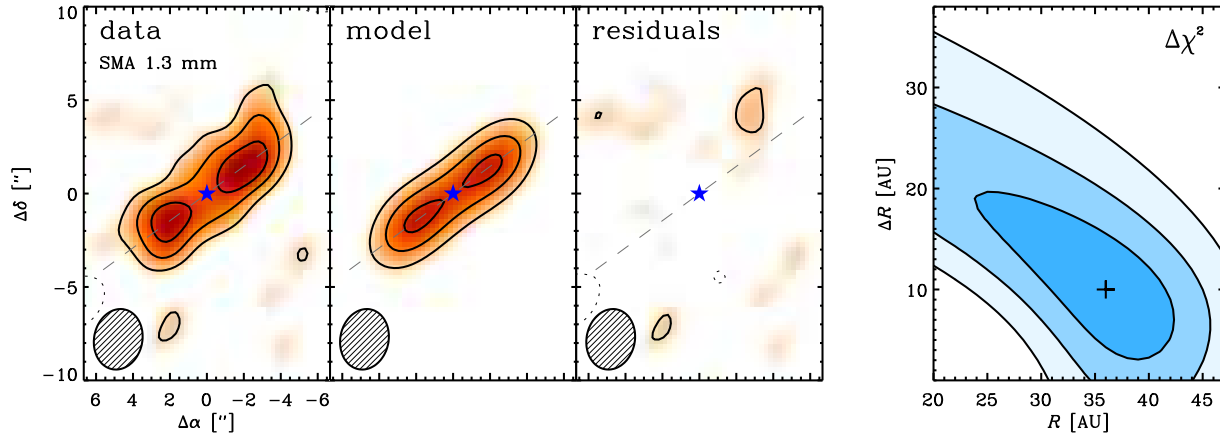


Fig. 2.— *Left panels:* SMA image of the 1.3 millimeter emission from AU Mic together with images of the best-fit axisymmetric belt model and residuals (see text). The contour levels and beam size are the same as in Figure 1. The dashed line indicates the 130° position angle of the scattered light disk. *Right panel:* The χ^2 surface for the model emission belt center and width parameters, with contours at $1, 2, 3\sigma$. The cross marks the best-fit model.

Table 1. Submillimeter Array Observations of AU Mic

Observation	2011 Jul 31	2011 Sep 26	2011 Sep 27	2011 Oct 25
Array Configuration	Extended	Compact	Compact	Compact
Number of Antennas	8	6	6	7
Baseline Lengths (m)	10–189	8–68	8–68	8–68
LO frequency (GHz)	235.6	225.4	225.4	235.6
225 GHz atm. opacity ^a	0.10	0.10–0.06	0.06	0.08

^aMeasured at the nearby Caltech Submillimeter Observatory.